HAL open science

Quasi-geostrophic modes in the Earth's fluid core with an outer stably stratified layer

Jérémie Vidal, Nathanaël Schaeffer

▶ **To cite this version:**

Jérémie Vidal, Nathanaël Schaeffer. Quasi-geostrophic modes in the Earth's fluid core with an outer stably stratified layer. 2015. insu-01110339v1

HAL Id: insu-01110339

https://insu.hal.science/insu-01110339v1

Preprint submitted on 27 Jan 2015 (v1), last revised 26 Jun 2015 (v2)

HAL is a multi-disciplinary open access archive for the deposit and dissemination of scientific research documents, whether they are published or not. The documents may come from teaching and research institutions in France or abroad, or from public or private research centers.

L'archive ouverte pluridisciplinaire **HAL**, est destinée au dépôt et à la diffusion de documents scientifiques de niveau recherche, publiés ou non, émanant des établissements d'enseignement et de recherche français ou étrangers, des laboratoires publics ou privés.

Distributed under a Creative Commons Attribution - NonCommercial - ShareAlike 4.0 International License

Quasi-geostrophic modes in the Earth's fluid core with an outer stably stratified layer

J. Vidal[1,2] and N. Schaeffer[1,2]

[1] Univ. Grenoble Alpes, ISTerre, F-38041 Grenoble, France
[2] CNRS, ISTerre, F-38041 Grenoble, France

January 27, 2015

Abstract

Seismic waves sensitive to the outermost part of the Earth's liquid core seem to be affected by a stably stratified layer at the core-mantle boundary. Such a layer could have an observable signature in both long-term and short-term variations of the magnetic field of the Earth, which are used to probe the flow at the top of the core. Indeed, with the recent SWARM mission, it seems reasonable to be able to identify waves propagating in the core with period of several months, which may play an important role in the large-scale dynamics.

In this paper, we characterize the influence of a stratified layer at the top of the core on deep quasi-geostrophic (Rossby) waves. We compute numerically the quasi-geostrophic eigenmodes of a rapidly rotating spherical shell, with a stably stratified layer near the outer boundary. Two simple models of stratification are taken into account, which are scaled with commonly accepted values of the Brunt-Väisälä frequency in the Earth's core.

In the absence of magnetic field, we find that both azimuthal wavelength and frequency of the eigenmodes control their penetration into the stratified layer: the higher the phase speed, the higher the permeability of the stratified layer to the wave motion. We also show that the theory developed by Takehiro and Lister (2001) for thermal convection extends to the whole family of Rossby waves in the core. Adding a magnetic field, the penetrative behaviour of the quasi-geostrophic modes (the so-called fast branch) is insensitive to the imposed magnetic field and only weakly sensitive to the precise shape of the stratification.

Based on these results, the large-scale and high frequency modes (1 to 2 month periods) may be detectable in the geomagnetic data measured at the Earth's surface, especially in the equatorial area where the modes can be trapped.

1 Introduction

The existence of a stably stratified layer at the top of the Earth's liquid core can have consequences on different aspects of the Earth's core dynamics. Such a layer can have a chemical origin with the accumulation of light elements coming from the growth of the inner core (Fearn and Loper, 1981; Braginsky, 2007; Gubbins and Davies, 2013) or from chemical interactions with the mantle if the outer part of the core is under-saturated in oxygen and silicium (Buffett and Seagle, 2010). It can also have a thermal origin, if the heat flux at the core mantle-boundary is lower than the adiabatic heat flux in the core. With their recent

estimations of the thermal iron conductivity in the Earth's core, de Koker et al. (2012) and Pozzo et al. (2012) claim that such a layer can be thermally stable at the top of the core.

The strength of the stratification in such a layer is characterized by the Brunt-Väisälä frequency

$$N = \sqrt{-\frac{g}{\rho}\frac{\mathrm{d}\rho}{\mathrm{d}r}}, \tag{1}$$

where $\rho(r)$ is the density profile as a function of the radius, and g the acceleration of gravity, which is considered constant in the thin layer (e.g. Crossley, 1984). A stably stratified layer corresponds to the case $N^2 > 0$, and a convective region to $N^2 < 0$. The comparison between N and the planetary rotation rate Ω allows to distinguish two stratification regimes: weak stratification when $N < 2\Omega$ and strong stratification when $N > 2\Omega$.

The presence of such a stratified layer at the top of the outer core has been advocated by some seismologists to explain travel-time anomalies of seismic body waves sensitive to the outermost part of the Earth's liquid core. It is however difficult to detect small density anomalies in this region, because body waves are also affected by the strong heterogeneities of the D" layer at the base of the mantle (Souriau, 2007). Optimistic estimations give a thickness of the stratified layer between 50-100 km (Lay and Young, 1990) and 300 km (Helffrich and Kaneshima, 2010), with a weak stratification corresponding to $N/2\Omega \sim 0.1$ in the latter case.

In a stratified layer, waves in which the Coriolis and buoyancy forces play an important role exist (Friedlander and Siegmann, 1982). These inertia-gravity waves have been investigated for several decades in the geophysical and astrophysical contexts (Olson, 1977; Crossley and Rochester, 1980; Crossley, 1984; Friedlander, 1985; Dintrans et al., 1999). If we could detect them, they would also provide evidence for the existence of a stably stratified layer in the outermost part of the Earth's core. The possible detection of these waves in the geodetic high frequency spectrum attracted attention some years ago, thanks to the development of superconducting gravimeters (Melchior and Ducarme, 1986; Aldridge and Lumb, 1987). Unfortunately, the observations in the high frequency range do not require a stably stratified layer to explain the data (Melchior et al., 1988), mainly because of the uncertainty on the frequencies of the waves (Rieutord, 1995). The evolution of the magnetic field of the Earth also gives constraints on the stratification at the top of the core (Gubbins, 2007).

Although still debated, and with characteristics such as depth and N not known, the existence of such a layer would give constraints on the thermal history of the core (Labrosse et al., 1997; Lister and Buffett, 1998; Labrosse, 2003). This layer may also modify the dynamics of the Earth's liquid core. Zhang and Schubert (1997), Takehiro and Lister (2001, 2002) and more recently Nakagawa (2011) studied the penetration of columnar convective motions of a rapidly rotating spherical shell in a stably stratified layer located at the outer boundary. Their results show that the stratification acts as an interface, which can be crossed by large-scale motions while small-scale ones are trapped below the layer when the stratification is strong enough. Such a layer has then the ability to partially hide geophysical flows inside the Earth's core, which has important implications for core flow inversion.

Indeed, using recordings of the magnetic field, it is possible to infer the flow at the core surface using inversion techniques (Holme, 2007). Assuming a quasi-geostrophic (columnar) flow, it is then possible to reconstruct the flow in the core interior (see e.g. Pais and Jault, 2008). Although there is evidence for quasi-geostrophic dynamics in the Earth's core (Gillet et al., 2011), the presence of a stratified layer may prevent us to reconstruct part of the interior flow (Bloxham, 1990). Moreover, a stratified layer can host its own eigenmodes, which may

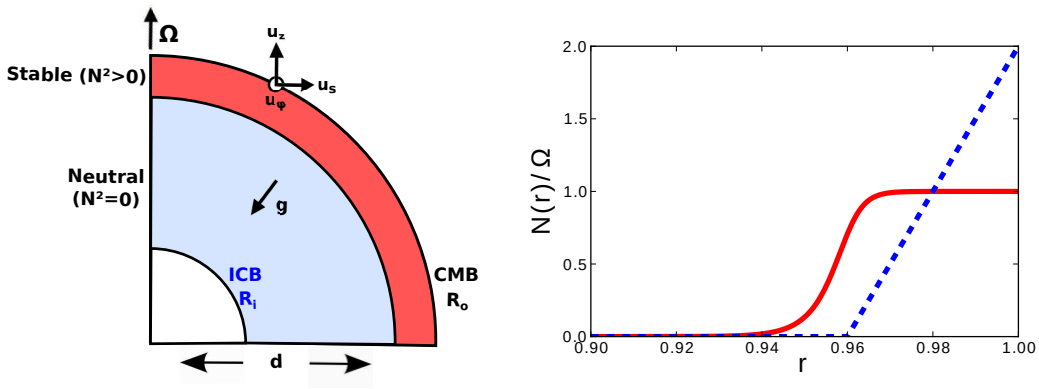

(a) (b)

Figure 1: (a) Geometry of the system. (b) Dimensionless Brunt-Väisälä frequency $N(r)/\Omega$ as a function of the dimensionless radius r. The solid red and dashed blue curves correspond to model (12) and model (13) respectively, with $N_0 = \Omega$. The thickness of the stratified layer is 140 km.

then be distinct from the flow in the bulk of the core (Braginsky, 1998, 1999; Buffett, 2014).

In this study, we characterize the effect of a stratified layer on otherwise quasi-geostrophic inertial modes in the Earth's core, also known as Rossby modes. Their time-scale is typically of a few months, and their signature may be actually seen in the geomagnetic data from the new SWARM mission (Olsen et al., 2013). Using a numerical eigenmode solver, we compute the linear hydromagnetic modes in a simplified model of the Earth's core including a stratified layer at the outer boundary. The effect of an imposed magnetic field on the modes is briefly considered in the case of a simple toroidal magnetic field depending only on the cylindrical radius s (Malkus, 1967).

The paper is divided as follows. Section 2 presents the mathematical modelling and section 3 the numerical methods used to solve the problem. The results are shown in section 4, with an emphasis on the shape of the eigenmodes and the dependence of their penetration length on governing parameters. Finally, section 5 discusses our findings.

2 Mathematical modelling

2.1 Basic equations

The geometry of the system is illustrated in the Figure 1a. We consider a rapidly rotating spherical shell of inner radius R_i and outer radius R_o, surrounded by perfectly insulating mantle and inner core. We assume an aspect ratio $\gamma = R_i/R_o = 0.35$, similar to that of the Earth's core. The shell, the mantle and the inner sphere are rotating at the same angular velocity $\mathbf{\Omega} = \Omega\,\hat{\mathbf{z}}$ aligned with the unitary vertical axis $\hat{\mathbf{z}}$ in cylindrical polar coordinates (s, ϕ, z). We work in the rotating reference frame attached to the mantle, in cylindrical polar coordinates or in spherical polar coordinates (r, θ, ϕ). The velocity $\mathbf{v}$, the magnetic field $\mathbf{B}$, the temperature T and the density ρ are subjected to small perturbations around a basic

state $(\mathbf{U_0}, \mathbf{B_0}, T_0, \rho_0)$. Let us write

$$[\mathbf{v}, \mathbf{B}]\,(\mathbf{r}, t) = [\mathbf{U_0}, \mathbf{B_0}]\,(\mathbf{r}) + [\mathbf{u}, \mathbf{b}]\,(\mathbf{r}, t), \tag{2}$$

$$T(\mathbf{r}, t) = T_0(r) + \Theta(\mathbf{r}, t), \tag{3}$$

$$\rho(\mathbf{r}, t) = \rho_0\,(1 - \alpha\Theta(\mathbf{r}, t))\,, \tag{4}$$

where α is the volume coefficient of thermal expansion and $(\mathbf{u}, \mathbf{b}, \Theta, -\rho_0\alpha\Theta)$ the perturbations of small amplitude. For the sake of simplicity, we impose $\mathbf{U_0}(\mathbf{r}) = \mathbf{0}$, which corresponds to a solid-body rotation in the inertial frame. We also assume that the background density ρ_0 is constant, neglecting the variations due to adiabatic compression across the shell (Rieutord, 1995). We take into account the density perturbation only in the gravity term with the Boussinesq approximation, considering a gravity field of the form $\mathbf{g} = -g_o r\,\hat{\mathbf{r}}$ with g_o the gravity field at the outer boundary and $\hat{\mathbf{r}}$ the unitary radial vector.

To keep the model simple, we suppose that the background magnetic field $\mathbf{B_0}$ in the shell is the Malkus field (Malkus, 1967)

$$\mathbf{B_0}(\mathbf{r}) = B_0\,\mathbf{b_0}(\mathbf{r}) = B_0\,r\sin\theta\,\hat{\boldsymbol{\phi}}. \tag{5}$$

It is a purely toroidal and azimuthal field which increases with the cylindrical radius $s = r\sin\theta$. This assumption is consistent with our choice for the background velocity, since no basic velocity $\mathbf{U_0}$ is needed for the basic state to be in equilibrium (the resulting Lorentz force is balanced by the pressure gradient).

We use R_o as the length scale, Ω^{-1} as the time scale, $\rho_0 R_o \Omega^2$ as the pressure scale, $\Omega^2 R_o/\alpha g_o$ as the temperature scale and $\sqrt{\mu_0\rho_0}\,\Omega R_o$ as the magnetic scale. As we are interested by the eigenmodes, we neglect the non-linear terms and the dimensionless equations satisfied by the perturbations are

$$\frac{\partial \mathbf{u}}{\partial t} + 2\,\hat{\mathbf{z}} \wedge \mathbf{u} = -\nabla P + Le\,[(\nabla \wedge \mathbf{b}) \wedge \mathbf{b_0} + (\nabla \wedge \mathbf{b_0}) \wedge \mathbf{b}] + r\Theta\,\hat{\mathbf{r}} + E\,\nabla^2\mathbf{u} \tag{6}$$

$$\frac{\partial \Theta}{\partial t} = -\frac{N^2(r)}{\Omega^2}\,\mathbf{u}\cdot\hat{\mathbf{r}} + \frac{E}{Pr}\nabla^2\Theta, \tag{7}$$

$$\frac{\partial \mathbf{b}}{\partial t} = Le\,\nabla \wedge (\mathbf{u} \wedge \mathbf{b_0}) + E_\eta\,\nabla^2\mathbf{b}. \tag{8}$$

Five governing parameters appear in the previous equations, namely the Ekman number E, the magnetic Ekman number E_η, the Prandtl number Pr, the Lehnert number Le and the dimensional Brunt-Väisälä frequency N. They are defined by

$$E = \frac{\nu}{\Omega R_o^2},\;\; E_\eta = \frac{\eta}{\Omega R_o^2},\;\; Pr = \frac{\nu}{\kappa},\;\; Le = \frac{B_0}{\sqrt{\rho_0\mu_0}\,\Omega R_o} \;\text{ and }\; N(r) = \sqrt{\alpha g_o \frac{\mathrm{d}T_0}{\mathrm{d}r}}, \tag{9}$$

with ν, κ and η respectively the viscous, thermal and magnetic diffusivities and B_0 the strength of the background magnetic field. In the computations, we take $Pr = 0.1 - 10$ and $Le = 10^{-4}$. Because of numerical constraints, we choose $E = E_\eta = 10^{-7}$.

Equations (6), (7) and (8) are completed with boundary conditions on the velocity, the temperature and the magnetic field. We impose on both shells the no-slip boundary condition for the velocity field

$$\mathbf{u} = \mathbf{0} \tag{10}$$

and an constant heat flux

$$\frac{\partial \Theta}{\partial r} = 0. \tag{11}$$

The magnetic field boundary conditions are the continuity of $\mathbf{b}$ and the continuity of the radial component of $\nabla \wedge \mathbf{b}$. The spherical harmonic expansion (introduced below) allows to write this as a boundary condition.

2.2 Basic state for the stratification

The Brunt-Väisälä frequency $N(r)$ in the core is highly speculative. Following Lister and Buffett (1998), let us assume that the spherical shell is divided in two parts (Figure 1a). A stably stratified layer with $N^2(r) > 0$ is located above a convective core of dimensionless radius d, which is supposed to be neutral with respect to the stratification ($N^2(r) = 0$). This assumption filters out the coupling between waves and convection (Rieutord, 1995). We set the radius $d = 0.96$, which corresponds to a stratified layer of thickness 140 -150 km. This thickness belongs to the range estimated by seismic studies (Helffrich and Kaneshima, 2010). It is also inferred by Buffett (2014) to match the geomagnetic secular variation with slow Magneto-Archimedes-Coriolis (MAC) waves. Following Takehiro and Lister (2001, 2002) and Nakagawa (2011), $N(r)$ is given by

$$N(r) = \sqrt{-\frac{N_0}{2}\left[1 - \tanh\left(\frac{r-d}{a}\right)\right] + N_0^2} \tag{12}$$

and is illustrated in Figure 1b. N_0 is the Brunt-Väisäla frequency at the outer boundary and $a = 0.005$ the transition thickness between the neutral core and the stratified layer. $N(r)$ is thus a smooth profile in the core with a roughly constant value $N(r) \simeq N_0$ in the outer layer. Different values of N_0 are taken into account. In addition, we also consider a profile similar to the one used by Rieutord (1995) and Buffett (2014), *i.e.*

$$N(r) = \begin{cases} 2N_0(r-d)/(1-d) & \forall\ r \geq d \\ 0 & \forall\ r < d \end{cases}. \tag{13}$$

It is linear in the stratified layer, with a mean value N_0 and a maximum value $2N_0$ at the outer boundary.

3 Numerical modelling

3.1 Spectral method

As they are solenoidal, $\mathbf{u}$ and $\mathbf{b}$ are decomposed into poloidal and toroidal parts

$$\mathbf{u} = \nabla \wedge \nabla \wedge (U\mathbf{r}) + \nabla \wedge (V\mathbf{r}), \tag{14}$$

$$\mathbf{b} = \nabla \wedge \nabla \wedge (G\mathbf{r}) + \nabla \wedge (H\mathbf{r}), \tag{15}$$

with (U, G) and (V, H) the poloidal and toroidal scalars. The scalars (U, V, G, H, Θ) are then expanded on orthonormalized spherical harmonics $Y_l^m(\theta, \phi)$, of degree l and order m, as

$$[U, V, \Theta]\,(\mathbf{r}, t) = \sum_{l=m}^{\infty} [U_l^m, V_l^m, \Theta_l^m]\,(r)\, Y_l^m(\theta, \phi) \exp(\lambda t), \tag{16}$$

$$[G, H,]\,(\mathbf{r}, t) = \sum_{l=m}^{\infty} [G_l^m, H_l^m]\,(r)\, Y_l^m(\theta, \phi) \exp(\lambda t). \tag{17}$$

Since the basic state $(\mathbf{U_0}, \mathbf{B_0})$ is axisymmetric, there is no coupling between Fourier modes m in the equations (6) to (8). Thus, one can seek solutions $(\mathbf{u}, \Theta, \mathbf{b})$ with a single azimuthal wavenumber m. As we are interested in the eigenmodes of the system, we assume that the time dependence of all perturbations is proportional to $\exp(\lambda t)$, with the complex eigenvalue

$$\lambda = \tau + i\omega \tag{18}$$

where τ is the growth rate of the mode and ω its frequency, both non-dimensional.

Thanks to the spectral decomposition, the boundary conditions are easy to express. On the two boundaries, the no-slip condition becomes

$$U_l^m = \frac{\mathrm{d}U_l^m}{\mathrm{d}r} = V_l^m = 0 \tag{19}$$

and the constant heat flux condition

$$\frac{\mathrm{d}\Theta_l^m}{\mathrm{d}r} = 0. \tag{20}$$

With the insulating boundary condition, the magnetic field matches a potential field in both the mantle and the inner sphere, resulting to

$$\frac{\mathrm{d}G_l^m}{\mathrm{d}r} - \frac{l}{r} G_l^m = H_l^m = 0 \tag{21}$$

on the inner boundary $(r = \gamma)$ and

$$\frac{\mathrm{d}G_l^m}{\mathrm{d}r} + \frac{l+1}{r} G_l^m = H_l^m = 0 \tag{22}$$

on the outer boundary $(r = 1)$.

3.2 Symmetry considerations

The equations (6 - 8) are symmetric or anti-symmetric with respect to the equatorial plane. This implies that solutions can be characterized by their symmetry with respect to the equator (Gubbins and Zhang, 1993).

In the following, we focus on equatorially symmetric $\mathbf{u}$ and Θ, because quasi-geostrophic flows have this equatorial symmetry. They satisfy

$$[u_r, u_\theta, u_\phi](r, \theta, \phi) = [u_r, -u_\theta, u_\phi](r, \pi - \theta, \phi), \tag{23}$$

$$\Theta(r, \theta, \phi) = \Theta(r, \pi - \theta, \phi). \tag{24}$$

Because $\mathbf{B_0}$ is symmetric, $\mathbf{b}$ is also symmetric with respect to the equatorial plane. According to the symmetry of Y_l^m, the spherical harmonic expansions for the poloidal and toroidal

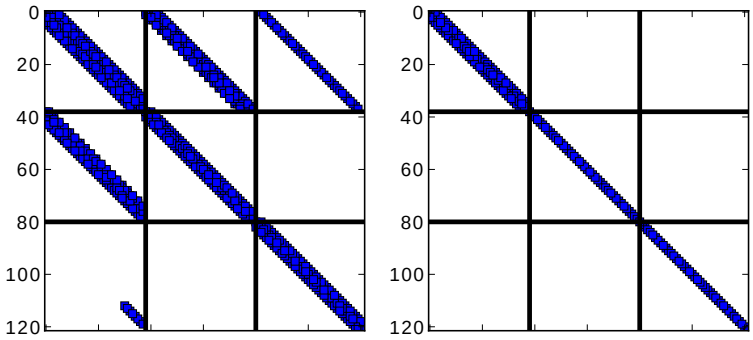

Figure 2: Sparse matrices A and B in the non-magnetic case. $L_{max} = 6$ and $N_r = 20$. The black lines separate the poloidal and toroidal components of the velocity and the temperature field. The first line of blocks represents the evolution equation of the poloidal component of the velocity (coupled to the toroidal flow by the Coriolis force and to the temperature by the Buoyancy force), the second line is the equation for the toroidal velocity, and the last line is the equation for the temperature (coupled to the poloidal flow only in the stratified layer).

components of $\mathbf{u}$ and $\mathbf{b}$ alternate to match the equatorial symmetry. Note also that the Coriolis force couples U_l^m and $V_{l\pm1}^m$. Following Schmitt (2010), the symmetric part of $\mathbf{u}$ and Θ is given by

$$(U_l^m, V_{l+1}^m, \Theta_l^m, G_l^m, H_{l+1}^m), \tag{25}$$

for a given azimuthal number m with $l = m, m+2, m+4, \ldots$

3.3 Numerical implementation

Substituting from (16) and (17) into the governing equations (6) to (8) leads to a set of linear differential equations which forms a generalized eigenvalue problem with its boundary conditions. To get numerical solutions, the spherical harmonic expansions are truncated at the harmonic degree L_M and the differential operators are represented by a second order finite difference scheme on an irregular mesh of N_r levels, adjusted to properly resolve the Ekman boundary layers. The eigenvalue problem is now in a matrix form as a complex, non-hermitian and generalized eigenvalue problem

$$A\mathbf{X} = \lambda B\mathbf{X}. \tag{26}$$

λ is the eigenvalue and $\mathbf{X}$ is the associated eigenvector given by

$$\mathbf{X} = \left(U_l^m(r_i), V_{l+1}^m(r_i), \Theta_l^m(r_i), G_l^m(r_i), H_{l+1}^m(r_i)\right)^t, \tag{27}$$

with $i = 0, 1, \ldots, N_r$ and $l = m, m+2, m+4, \ldots$ for the symmetric eigenmodes. The two matrices A and B, collecting the terms on the left-hand side and right-hand side of the equations, have approximately $(5L_M N_r/2)^2$ elements. In order to have good spatial and spectral resolutions, we use $L_M \sim 350$ and $N_r \simeq 850$ for Ekman number $E = 10^{-7}$. Matrices A and B have a large number of elements, but most of them are zero. They are stored as sparse matrices in order to reduce the required memory (see Figure 2).

m	n_c	ω		
		$N_0 = 0$	$N_0 = \Omega$	$N_0 = 2\,\Omega$
1	8	-4.6×10^{-3}	-5.1×10^{-3}	-5.4×10^{-3}
	3	-1.4×10^{-2}	-1.7×10^{-2}	-2.0×10^{-2}
3	13	-3.9×10^{-3}	-4.4×10^{-3}	-4.8×10^{-3}
	7	-1.9×10^{-2}	-2.0×10^{-2}	-2.3×10^{-2}
6	13	-6.9×10^{-3}	-7.5×10^{-3}	-8.0×10^{-3}
	8	-2.1×10^{-2}	-2.4×10^{-2}	-2.9×10^{-2}
8	14	-7.9×10^{-3}	-8.4×10^{-3}	-9.3×10^{-3}
	10	-1.8×10^{-2}	-2.0×10^{-2}	-2.2×10^{-2}

Table 1: Wave number m, approximative number of quasi-geostrophic columns n_c, dimensionless frequency ω and period in months of some numerical eigenmodes for three values of N_0, without magnetic field. Computations at $E = 10^{-7}$ and $Pr = 0.1$. $N(r)$ is given by (12).

Following Rieutord et al. (1997) and Dintrans et al. (1999), the linear eigenvalue problem (26) is solved using the shift-and-invert spectral transformation: instead of solving the problem (26), the related problem

$$(A - \sigma B)^{-1} B\mathbf{X} = \mu\mathbf{X} \tag{28}$$

is solved with σ the shift and the new eigenvalue μ related to λ by

$$\mu = \frac{1}{\lambda - \sigma}. \tag{29}$$

With this spectral transformation, it is easier to get the least damped quasi-geostrophic modes, imposing $\sigma = i\omega$ with $\omega \ll 1$. Only eigenvalues with absolute residuals $|(A - \sigma B)^{-1} B\mathbf{X} - \mu\mathbf{X}| < 10^{-12}$ are accepted as good eigenvalues.

We wrote a Python code, nicknamed *Singe* (Spherical INertia-Gravity Eigenmodes), that relies on the `SLEPc` library (Hernandez et al., 2005) to solve the eigenvalue problem using the restarted Krylov-Schur method (Hernandez et al., 2009) together with the shift-and-invert strategy. `SLEPc` is an open-source scientific library developed to efficiently solve large and sparse eigenvalue problems on parallel computers. It is itself based on `PETSc` (Balay et al., 1997, 2014), another open-source library intended to solve scientific problems modelled by partial differential equations. Finally, *Singe* uses the `SHTns` library (Schaeffer, 2013) for the spherical harmonic transforms.

The *Singe* code was benchmarked with the theoretical solutions of Zhang et al. (2001), Liao et al. (2001) and Zhang et al. (2003) in the full sphere. As benchmarks for the spherical shell geometry, we used the numerical results of Rieutord et al. (1997) without stratification and of Dintrans et al. (1999) with a constant stratification in the shell.

Singe is available at `https://bitbucket.org/nschaeff/singe` as free software.

4 Results

4.1 Description of eigenmodes

To study the behaviour of quasi-geostrophic inertial modes in the presence of a stratified layer, we first focus on the non-magnetic case. Characteristics of some modes are gathered in Table

1. Each mode is specified by a triplet (ω, m, n_c), with m the azimuthal wave number and n_c the number of quasi-geostrophic columns within the shell. The dimensionless frequency ω, with corresponding periods ranging from one to several months, is always negative because the eigenmodes propagate westwards. It is a characteristic of Rossby waves. Indeed, looking at the different forces, we find that the modes are dominated by the Coriolis force, with some exceptions in the stably stratified layer (see below). The Coriolis force tends to align the flow along the spin axis to create Taylor columns, and the modes are mainly quasi-geostrophic inertial modes (almost invariant along the rotation axis). The frequency depends also on the length scale of the modes. For a given azimuthal number m, high frequency modes are large scale modes with a small number of columns n_c, while low frequency are small scale modes with a large number of columns.

The precise shape of the modes depends on the stratification, which may influence the penetration of the flow in the outer layer (Zhang and Schubert, 1997; Takehiro and Lister, 2001). However, the overall pattern of the modes in the neutral part of the core smoothly evolves with the stratification strength N_0. For commonly accepted values of the Brunt-Väisälä frequency N_0, the number of columns of a mode remains approximatively the same, while the exact position and thickness of the columns change near the outer layer. A smooth increase of N_0 allows us to study the evolution of the modes. It can be done with an iterative process to follow a given mode defined by (m, n_c). As observed in Table 1, ω slowly increases with N_0.

The cylindrical components u_s and u_ϕ in the equatorial plane of some modes are shown in Figure 3. It is worth noting that lower frequency modes are spiralling more than higher frequency modes. The spiralling appears because the viscosity is overestimated in our computations (see appendix A for more details). Finally, the kinetic energy is dominated by the azimuthal component of the velocity u_ϕ, which is more concentrated in the equatorial region when the frequency is higher. This phenomenon, called trapping, is known for inertial waves (Zhang, 1993) as well as for inertia-gravity waves (Crossley, 1984; Friedlander, 1985). When $E < 10^{-7}$, we observe that this trapping becomes more efficient. Unfortunately, it is then expensive to resolve numerically, because it needs enough grid points to capture the boundary layer and enough spherical harmonics to describe the trapping. For these reasons, we set the Ekman number to 10^{-7} in our computations.

Let us now switch on the background magnetic field $\mathbf{B_0}$ given by expression (5). Without stratification, a background magnetic field splits the modes into "slow" and "fast" magneto-Coriolis (MC) waves, the latter being essentially pure inertial waves (see e.g. Zhang et al., 2003). With a Lehnert number $Le = 10^{-4}$ (which is in the range estimated for the Earth's core), and with $E = E_\eta = 10^{-7}$, $Pr = 0.1$, the frequency ω changes by less than 1% and the shape of the modes are very similar to the ones obtained without magnetic field. This holds for every eigenmode considered here and for all values of the Brunt-Väisälä frequency N_0 investigated here. It shows that the eigenmodes considered in this study are barely modified by the background magnetic field, because they are mainly "fast" quasi-geostrophic inertial modes. These results are in agreement with the theoretical predictions of Malkus (1967) and Zhang et al. (2003) for a homogeneous fluid contained in a full sphere. Furthermore, Canet et al. (2014) considered a quasi-geostrophic model of magneto-Coriolis (MC) waves and showed that various shapes of a toroidal background magnetic fields do not affect the fast modes either.

Since our quasi-geostrophic modes are not affected significantly by the magnetic field, with or without a stratified layer, we will no longer consider the magnetic field in the remainder

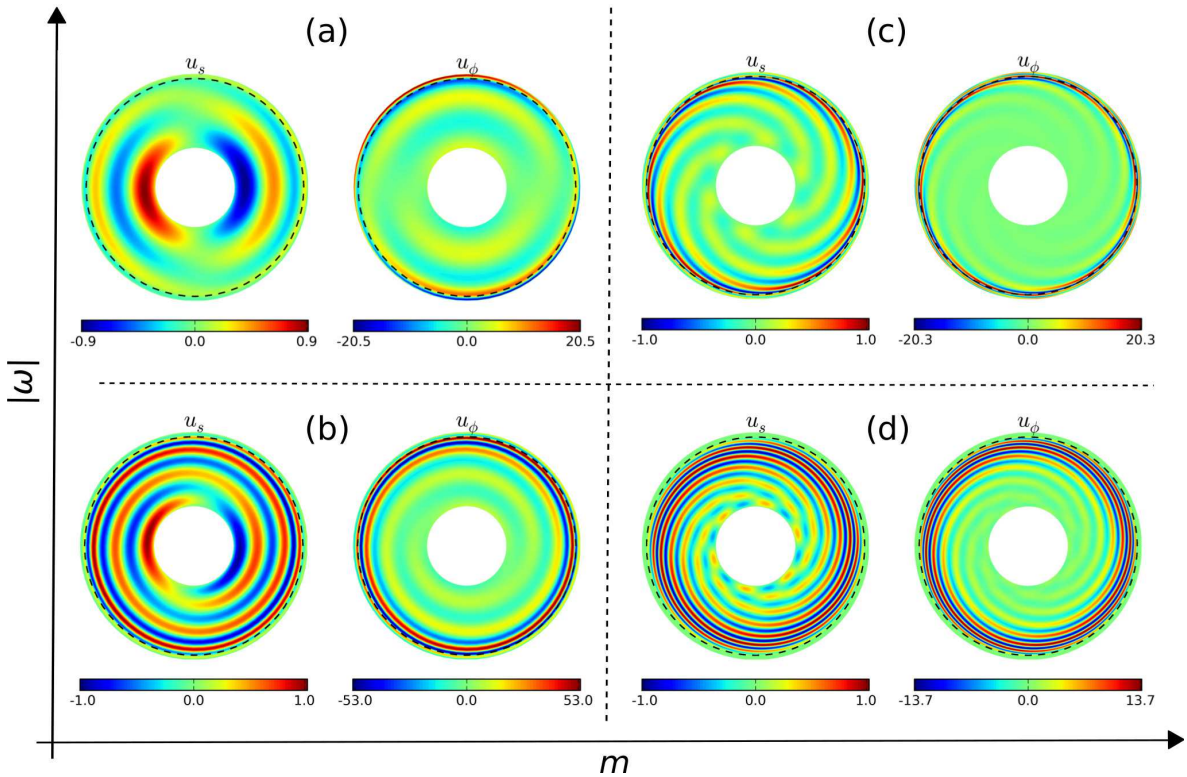

Figure 3: Contours of the cylindrical components u_s and u_ϕ of four numerical eigenmodes from Table 1 (without magnetic field) in the plane $(m, |\omega|)$. ω is the dimensionless frequency. Contours are shown in the equatorial plane as seen from above. The vertical component u_z is not shown because it vanishes in the equatorial plane. The velocity is normalized by the maximum value of u_s. The black dashed curve represents the transition between the neutral core and the stably stratified layer. The modes were computed at $E = 10^{-7}$ and $Pr = 0.1$. $N(r)$ is given by (12) and $N_0 = \Omega$. (a) High-frequency mode $m = 1$. (b) Low-frequency mode $m = 1$. (c) High-frequency mode $m = 6$. (d) Low-frequency mode $m = 6$.

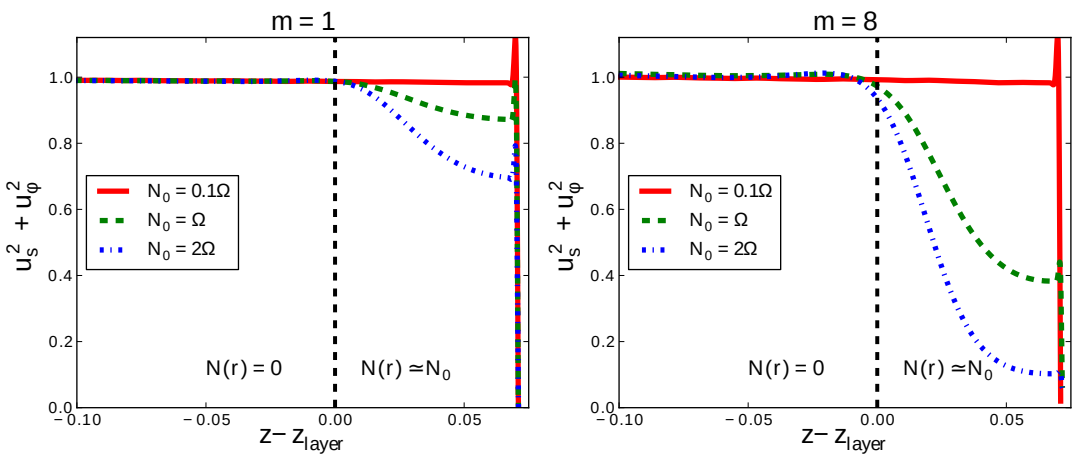

Figure 4: Distribution of the azimuthal average of the quasi-geostrophic kinetic energy $u_s^2+u_\phi^2$, along a quasi-geostrophic column located near the cylindrical radius $s = 0.7$, for some high frequency modes of the Table 1, computed at $E = 10^{-7}$ and $Pr = 0.1$. $N(r)$ is given by eq. (12). The horizontal axis $z - z_{layer}$ represents the difference between the vertical coordinte z along the column and the coordinate of the bottom of the stratified layer z_{layer}. The vertical dashed line shows the transition between the neutral core and the stably stratified layer. For each m, the modes have approximately the same shape in the neutral core. The bumps in the energy at the right-hand side of the curves show the effect of the Ekman pumping. The curves are normalized by the value of their energy in the equatorial plane (not shown).

of this paper, effectively solving only equations (6) and (7) with $Le = 0$. This simplifies the numerical study quite a bit. Note that although the fast branch considered here is unaffected, the slow branch will most certainly be affected by the magnetic field, but this is beyond the scope of this paper.

4.2 Penetration into the stratified layer

In order to quantify the penetration of the quasi-geostrophic modes into the stratified layer, we compute profiles at a given distance s from the rotation axis. Figure 4 shows the profiles of the azimuthal average of the quasi-geostrophic kinetic energy $u_s^2 + u_\phi^2$ along the axial direction, for three values of N_0 and two wave numbers m. For a given N_0, the modes have approximately the same frequency. The points are chosen along the column located at the cylindrical radius $s = 0.7$, where the energy is non-zero in the equatorial plane. The sharp bump before the decrease of the kinetic energy, observed on all curves, corresponds to the Ekman layer. When $N_0 = 0.1\,\Omega$, the Taylor column penetrates into the outer layer. The flow just below the Ekman layer is nearly the same as that in the neutral core. When $N_0 = \Omega$, the kinetic energy decreases in the layer, although it does not vanish before the Ekman layer is reached. When $N_0 = 2\,\Omega$, the kinetic energy is further reduced, and even more so for higher azimuthal modes m.

From these profiles (Fig. 4), we can define a transmission coefficient T. It is our key parameter to compare quantitatively the penetration of the flow inside the stably stratified outer layer, for eigenmodes of various shapes and frequencies. Let us define T as the ratio of

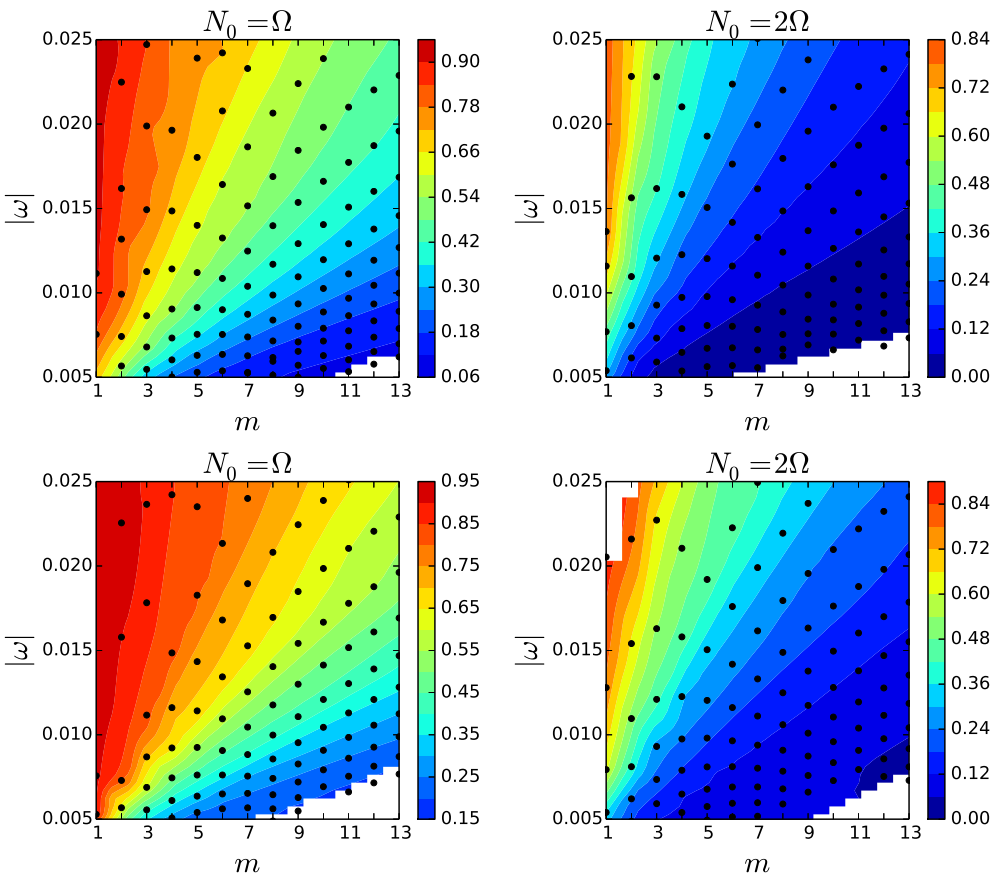

Figure 5: Maps of the amplitude of the transmission coefficient T as a function of the azimuthal number m and the dimensionless frequency $|\omega|$ of the modes. Top row: layer with constant Brunt-Väisälä frequency (eq. 12); bottom row: layer with linear Brunt-Väisälä frequency (eq. 13). The Brunt-Väisälä frequency is set to $N_0 = \Omega$ on the left column and $N_0 = 2\Omega$ on the right column. Values are computed at the cylindrical radius $s = 0.7$. T is interpolated between the black dots which represent numerical modes for which there are quasi-geostrophic columns at s where the kinetic energy is non-zero. In the two models, the stratified layer has the same thickness (140 - 150 km).

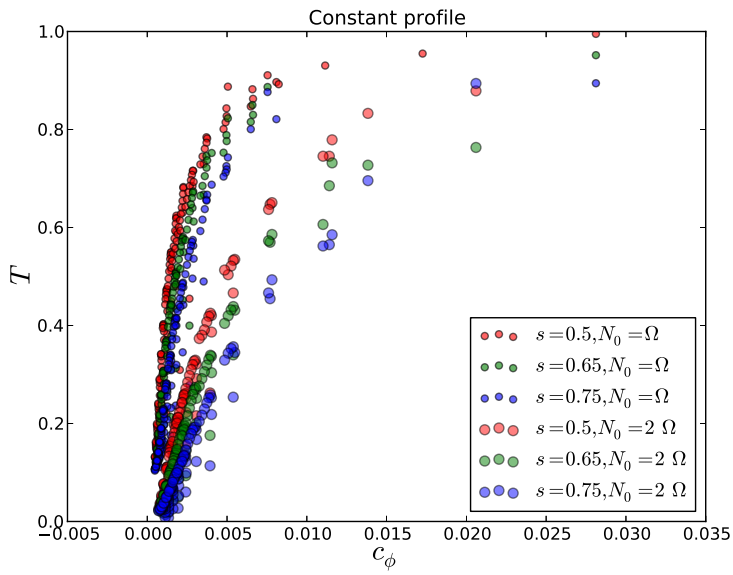

Figure 6: Dependence of transmission coefficient T with the dimensionless phase velocity $c_\phi = |\omega|/m$ of the modes, for various cylindrical radius s and Brunt-Väisälä frequency N_0. Computations were performed at $E = 10^{-7}$, $Pr = 0.1$ and $N_0 = \Omega$. T is computed automatically for all the modes. Only the results for constant Brunt-Väisälä frequency (eq. 12) are shown.

the value of the square root of the azimuthal average of the quasi-geostrophic kinetic energy $u_s^2 + u_\phi^2$, taken just under the Ekman boundary layer (Figure 4), to that in the equatorial plane. Figure 5 shows the distribution of transmission coefficients T defined along the quasi-geostrophic column at a given cylindrical radius ($s = 0.7$). Modes of different m and different frequencies ω are represented. For a given N_0, large-scale modes are less affected than small-scale modes which cannot penetrate deep into the layer. This behaviour is reinforced when N_0 increases, showing that the stratification clearly acts as a low-pass filter: large-scale eigenmodes (high frequencies, high m) penetrate deeper inside the outer layer than small-scale eigenmodes (low frequencies, large m).

Because $N(r)$ is not known in the Earth's core, Figure 5 also compares the effect of two stratification profiles (12) and (13). The modes can penetrate slightly deeper in the layer with the linear profile, but the overall distribution is similar. Therefore, the exact shape of $N(r)$ does not seem to affect the leading order behaviour for a layer with a given thickness. Finally, we have also observed that the thicker the layer, the less the modes penetrate into the outer layer, which is the expected behaviour.

The lines of constant transmission coefficient T displayed in Figure 5 suggest that a single parameter may control T. Figure 6 shows the transmission coefficient T as a function of the dimensionless angular phase velocity $c_\phi = |\omega|/m$ for profiles taken on modes with various m and ω, three cylindrical radii s, and two values of N_0. The modes with different m and ω collapse quite well, although a residual dependence on s (the location of the quasi-geostrophic column in the shell) and N_0 is now apparent. Columns at high and mid latitudes can penetrate slightly better in the outer layer than columns at low latitudes. At a given s, modes with a

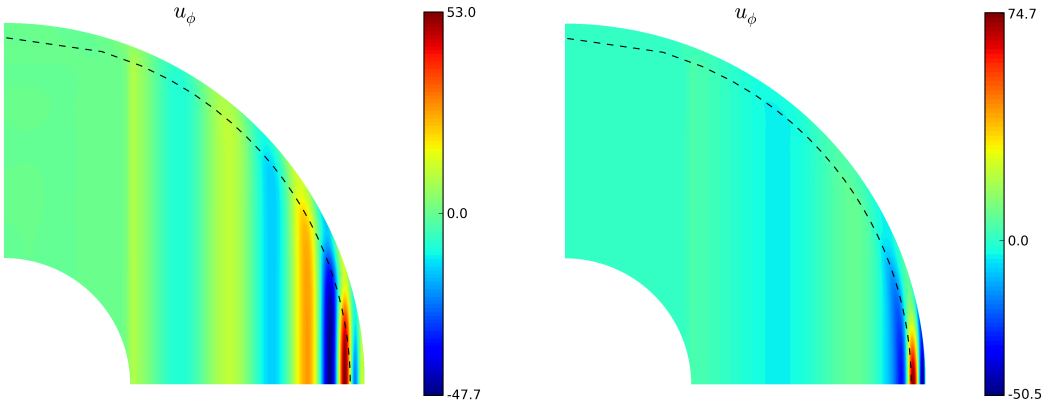

$N_0 = \Omega$
$\omega = -0.0115$

$N_0 = 2\Omega$
$\omega = -0.0138$

Figure 7: Distribution of the azimuthal component u_ϕ of the velocity field for two large-scale eigenmodes $m = 1$ in a meridional plane. The dashed line represents the bottom of the stratified layer. The amplitude is arbitrary. Computations at $E = 10^{-7}$ and $Pr = 0.1$.

larger phase velocity are in general less affected by the outer layer than the others. There are also some departures from the general trend, which are likely to come from the automatic procedure to follow modes as the parameters are changed and the automatic evaluation of T.

4.3 Equatorial trapping

A peculiar behaviour is observed near the equator. There, we observe that modes of dimensionless frequency $|\omega| \gtrsim 0.02$ and of small wave numbers $m \leq 3$ can penetrate inside the equatorial region, where the azimuthal component u_ϕ can be equatorially trapped in the stably stratified layer. This phenomenon is illustrated in Figure 7. In this case, the modes still have $\omega < 0$, reminding of Rossby waves, but they are now governed by both Coriolis and buoyancy forces. This trapping has been predicted by theoretical studies (Friedlander and Siegmann, 1982; Crossley, 1984). Note however that a strong dipolar magnetic field may release the trapped modes (Bergman, 1993).

4.4 Thermal vs chemical stratification

Thermal and chemical buoyancy are governed by the same advection-diffusion equations, the main difference being the very different value of their respective diffusivity. Estimates of diffusivities in the Earth's core suggest that representative values of Prandtl number are $Pr \gtrsim 0.1$ for thermal diffusivity and $Pr \gtrsim 10$ for the diffusivity of light elements in the core. We can thus study the effect of thermal or chemical stratification by adjusting the value of the Prandtl number in our model. Figure 8 shows the dependence of the absolute dimensionless frequency $|\omega|$ and of the transmission coefficient T as a function of Pr, for some high frequency modes of different wave numbers m. For $Pr > 10$, an asymptotic regime is reached where both ω and T do not depend on Pr any more. In any case, Pr has only a small effect on the penetration of the columns in the outer layer.

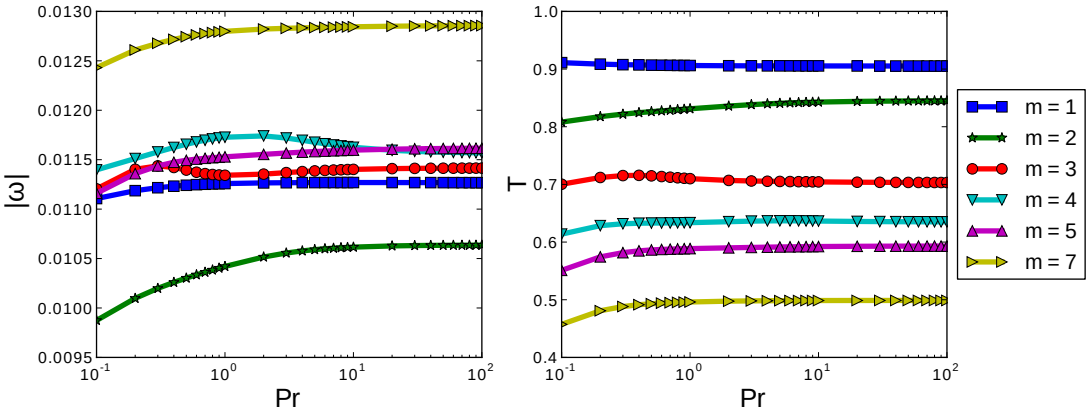

Figure 8: Evolutions of the absolute dimensionless frequency $|\omega|$ and of the transmission coefficient T as a function of the Prandtl number Pr of some quasi-geostrophic modes. Computations at fixed $E = 10^{-7}$ and for model (12) with $N_0 = \Omega$.

5 Discussion

5.1 Comparison with previous studies

We have shown that a sufficiently stratified layer can affect the penetration of quasi-geostrophic inertial modes based on their phase speed. A theoretical value for the penetration distance δ has been derived by Takehiro and Lister (2001), using a local plane layer approximation,

$$\delta_{th} = \frac{2\Omega}{N_0} \frac{1}{\sqrt{k^2 + l^2}} \tag{30}$$

where k and l are the wavenumbers in the azimuthal and radial directions respectively. Because l is difficult to estimate, they further simplify their expression assuming isotropy $l = k = m/s$ for a global neutral convection mode of azimuthal wavenumber m. They find good agreement between the penetration length obtained in numerical simulations and their estimate

$$\delta_m = \frac{2\Omega}{N_0} \frac{s}{\sqrt{2}\, m}, \tag{31}$$

as long as $\delta \lesssim 0.4$. However, this last expression δ_m translates into a transmission coefficient T that depends only on the azimuthal wavenumber m, in contradiction with our findings that also exhibit a strong dependence with the frequency ω (see Fig. 5).

We have found it difficult to measure reliably a penetration distance δ on the profiles shown on Figure 4, where the amplitude seems to decay exponentially in the lower region of the layer and then saturate to a constant value near the solid boundary. We therefore defined a transmission coefficient, which has the drawback of being dependent of the layer thickness, but the advantage of being well defined, even for arbitrarily shaped profiles.

The modes we have studied are very close to global Rossby modes, which have the following dispersion relation in a local plane approximation without stratified layer (Greenspan, 1968):

$$\omega = 2\Omega\beta \frac{k}{k^2 + l^2} \tag{32}$$

where $\beta = -s/(1-s^2)$ for a full sphere. Ignoring the small variations of ω with N (see table 1), we can use this expression to estimate $k^2 + l^2$ from ω and $k = m/s$. Equation (30) then becomes

$$\delta_{Rossby} = \frac{1}{N_0}\sqrt{2\Omega(1-s^2)\,\frac{|\omega|}{m}} = \frac{\cos(\theta)}{N_0}\sqrt{2\Omega\,|c_\phi|}, \tag{33}$$

where θ is the colatitude and c_ϕ the phase speed in the azimuthal direction. As shown on Figure 9, this last expression for δ that assumes the local dispersion relation of Rossby waves (eq. 32) seems to control all the variability in the transmission coefficient T.

We have thus shown that the local plane-layer theory of Takehiro and Lister (2001) for thermal convection extends to the whole family of Rossby waves (quasi-geostrophic inertial waves) in the core. This implies a transmission coefficient T for Rossby waves that depend only on phase speed $c_\phi = \omega/m$ and on colatitude θ in addition to the control parameters N_0 and Ω.

5.2 Possible observations in the geomagnetic data

It is worth noting that the the absolute frequency of the waves increases with N_0 (Table 1). This sensitivity of eigenmode frequencies to the Brunt-Väisäla frequency may be a way to probe for the existence of a stably stratified layer below the core-mantle boundary. Moreover, we expect maximum magnetic signatures of large-scale ($m < 3$) and high frequency modes (periods shorter than two months) in the equatorial area, where they are trapped.

Such high frequencies are very difficult to extract from the residual noise in the current geomagnetic models. However, the ability of the three SWARM satellites to better separate external and internal fields (Olsen et al., 2013), may enable us to detect the signature of these modes in the geomagnetic data.

5.3 Towards MAC waves

The studied quasi-geostrophic modes are only very weakly sensitive to the simple toroidal Malkus field, for magnetic field strength in the estimated range for the Earth's core ($Le = 10^{-4}$). It comes from the fact that these modes evolve on a time scale much faster than that of the Alfvén waves. A preliminary study with an axial field $\mathbf{B_0} = B_0\,\hat{\mathbf{z}}$ also shows that such a simple poloidal field does not play a significant role, neither on the frequency of the modes, nor on their ability to penetrate the stratified layer. We expect that these results remain valid with more complex magnetic fields. Unfortunately, our numerical code *Singe* is not well suited to take into account complex imposed fields, because they lead to an increasing number of coupled harmonic degrees, which are cumbersome to express and translate into matrix coefficients. A possible solution would be to use computed algebra systems (CAS) to write down the coupling operators between spherical harmonics in a symbolic way (as in Schmitt, 2010), and then to export them into a language suitable for numerical computations. Another more flexible approach is to use so-called matrix-free methods, which avoid to explicitly define the matrices, but require to provide appropriate preconditioners. These methods may come forward in the forthcoming years.

Acknowledgments The authors would like to thank the whole geodynamo team for fruitful discussions. Plots were produced using matplotlib (Droettboom et al., 2014). ISTerre is part of Labex OSUG@2020 (ANR10 LABX56).

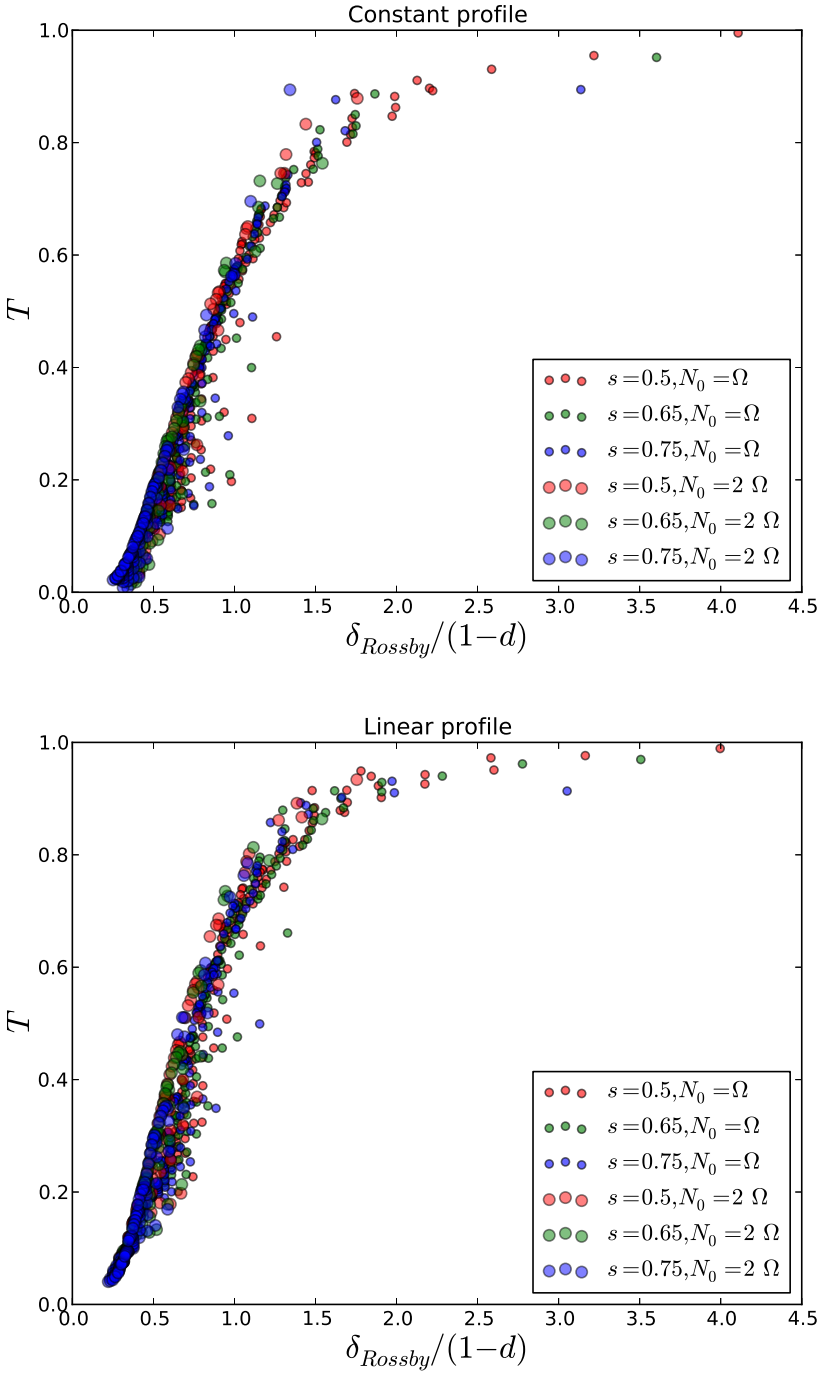

Figure 9: Transmission coefficient T as a function of theoretical penetration depth δ_{Rossby} (equation 33), normalized by the stratified layer thickness $1-d$. Top: constant stratification profile (eq. 12). Bottom: linear stratification profile (eq. 13). All transmission coefficients obtained for various position ($s = 0.5$, $s = 0.65$, $s = 0.75$) and two stratification strength ($N = \Omega$ and $N = 2\Omega$) collapse quite well.

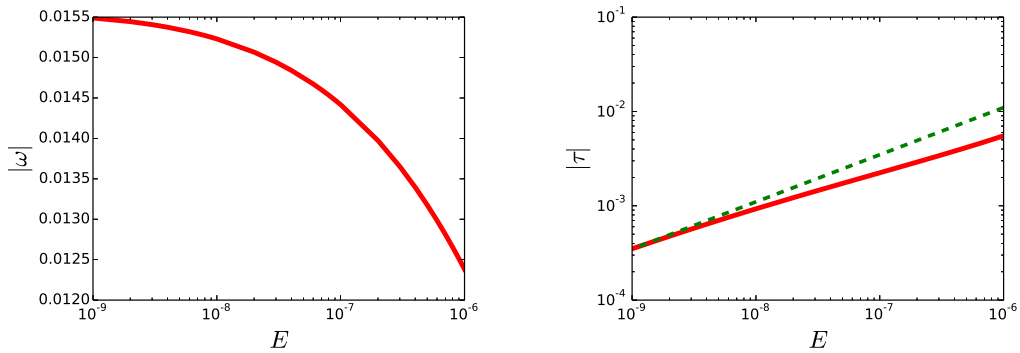

Figure 10: Frequency and damping rate of the quasi-geostrophic pure inertial mode with $m = 3$, as a function of the Ekman number. The green dashed line correspond to an $E^{1/2}$ scaling, the expected asymptotic damping due to the Ekman layers in a full sphere (Liao et al., 2001).

A Effect of viscosity on quasi-geostrophic inertial modes

Our study includes a small viscosity, which results in a non-zero damping of the modes, a small effect on their frequency, but also a significant effect on their shape, which is spiraling in the presence of sufficient viscosity.

As shown in Figure 10, the asymptotic frequency and damping rate are approached only when $E \sim 10^{-9}$. Coincidentally, Figure 11 shows that the spiralling shape vanishes at the same very low Ekman number. This shows that very low Ekman numbers are needed to have an asymptotic structure of quasi-geostrophic inertial waves.

References

Aldridge, K. and Lumb, L. (1987). Inertial waves identified in the earth's fluid outer core. *Nature*.

Balay, S., Adams, M. F., Brown, J., Brune, P., Buschelman, K., Eijkhout, V., Gropp, W. D., Kaushik, D., Knepley, M. G., McInnes, L. C., Rupp, K., Smith, B. F., and Zhang, H. (2014). PETSc Web page. `http://www.mcs.anl.gov/petsc`.

Balay, S., Gropp, W. D., McInnes, L. C., and Smith, B. F. (1997). Efficient management of parallelism in object oriented numerical software libraries. In Arge, E., Bruaset, A. M., and Langtangen, H. P., editors, *Modern Software Tools in Scientific Computing*, pages 163–202. Birkhäuser Press.

Bergman, M. I. (1993). Magnetic rossby waves in a stably stratified layer near the surface of the earth's outer core. *Geophysical & Astrophysical Fluid Dynamics*, 68(1-4):151–176.

Bloxham, J. (1990). On the consequences of strong stable stratification at the top of earth's outer core. *Geophysical Research Letters*, 17(12):2081–2084.

Braginsky, S. I. (1998). Magnetic rossby waves in the stratified ocean of the core, and topographic core-mantle coupling. *Earth Planets Space*, 50(8):641–649.

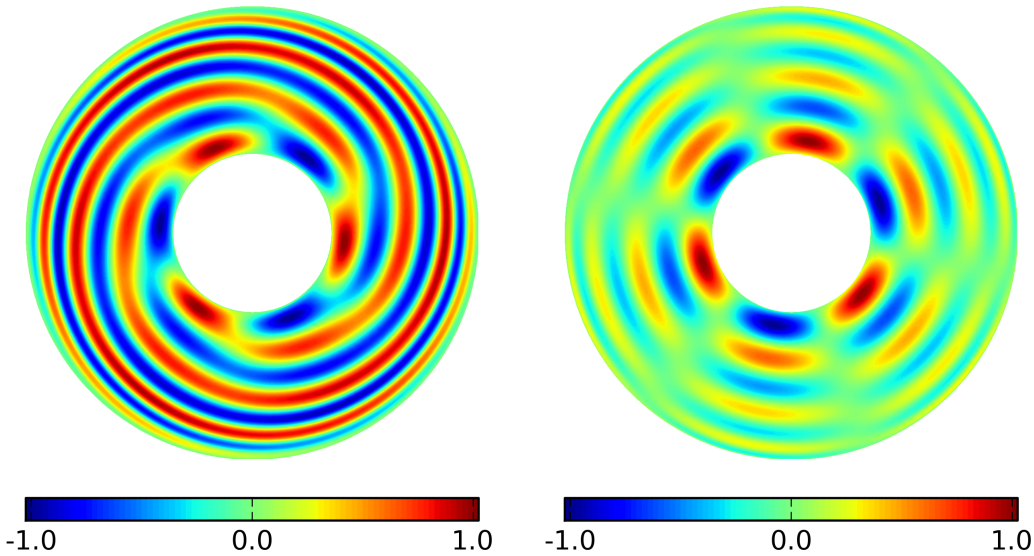

Figure 11: Equatorial cross-section of the quasi-geostrophic pure inertial mode with $m = 3$ with a small viscosity. Left $E = 10^{-6}$; right $E = 10^{-9}$.

Braginsky, S. I. (1999). Dynamics of the stably stratified ocean at the top of the core. *Physics of the earth and planetary interiors*, 111(1):21–34.

Braginsky, S. I. (2007). Formation of the stratified ocean of the core: a ternary alloy model. *Earth and Planetary Science Letters*, 253(3):507–512.

Buffett, B. A. (2014). Geomagnetic fluctuations reveal stable stratification at the top of the earth's core. *Nature*, 507:484–487.

Buffett, B. A. and Seagle, C. T. (2010). Stratification of the top of the core due to chemical interactions with the mantle. *Journal of Geophysical Research: Solid Earth*, 115(B4).

Canet, E., Finlay, C., and Fournier, A. (2014). Hydromagnetic quasi-geostrophic modes in rapidly rotating planetary cores. *Physics of the Earth and Planetary Interiors*, 229(0):1 – 15.

Crossley, D. (1984). Oscillatory flow in the liquid core. *Physics of the earth and planetary interiors*, 36(1):1–16.

Crossley, D. and Rochester, M. (1980). Simple core undertones. *Geophysical Journal International*, 60(2):129–161.

de Koker, N., Steinle-Neumann, G., and Vlček, V. (2012). Electrical resistivity and thermal conductivity of liquid fe alloys at high p and t, and heat flux in earth's core. *Proceedings of the National Academy of Sciences*, 109(11):4070–4073.

Dintrans, B., Rieutord, M., and Valdettaro, L. (1999). Gravito-inertial waves in a rotating stratified sphere or spherical shell. *Journal of Fluid Mechanics*, 398:271–297.

Droettboom, M., Hunter, J., Firing, E., Caswell, T. A., Dale, D., Elson, P., Lee, J.-J., McDougall, D., Straw, A., Root, B., Seppänen, J. K., May, R., Varoquaux, Yu, T. S., Moad, C., Nielsen, J. H., Gohlke, C., Würtz, P., Ivanov, P., Whitaker, J., Giuca, M., Hobson, P., mmetz bn, Evans, J., Cimarron, Thomas, I., dhyams, Hisch, T., NNemec, and jaytmiller (2014). matplotlib: v1.4.2.

Fearn, D. and Loper, D. E. (1981). Compositional convection and stratification of earth's core.

Friedlander, S. (1985). Internal oscillations in the earth's fluid core. *Geophysical Journal International*, 80(2):345–361.

Friedlander, S. and Siegmann, W. L. (1982). Internal waves in a rotating stratified fluid in an arbitrary gravitational field. *Geophysical & Astrophysical Fluid Dynamics*, 19(3-4):267–291.

Gillet, N., Schaeffer, N., and Jault, D. (2011). Rationale and geophysical evidence for quasi-geostrophic rapid dynamics within the earth's outer core. *Physics of the Earth and Planetary Interiors*, 187(3-4):380–390.

Greenspan, H. P. (1968). *The theory of rotating fluids*. Cambridge University Press.

Gubbins, D. (2007). Geomagnetic constraints on stratification at the top of earth's core. *Earth, Planets, and Space*, 59(7):661–664.

Gubbins, D. and Davies, C. (2013). The stratified layer at the core–mantle boundary caused by barodiffusion of oxygen, sulphur and silicon. *Physics of the Earth and Planetary Interiors*, 215:21–28.

Gubbins, D. and Zhang, K. (1993). Symmetry properties of the dynamo equations for palaeomagnetism and geomagnetism. *Physics of the earth and planetary interiors*, 75(4):225–241.

Helffrich, G. and Kaneshima, S. (2010). Outer-core compositional stratification from observed core wave speed profiles. *Nature*, 468(7325):807–810.

Hernandez, V., Roman, J. E., Tomas, A., and Vidal, V. (2009). Krylov-schur methods in SLEPc. Technical Report STR-7, Universitat Politècnica de València. Available at http://www.grycap.upv.es/slepc.

Hernandez, V., Roman, J. E., and Vidal, V. (2005). SLEPc : A scalable and flexible toolkit for the solution of eigenvalue problems. *ACM Trans. Math. Software*, 31(3):351–362.

Holme, R. (2007). *Large Scale Flow in the Core. In: Treatise in Geophysics, Geomagnetism, Vol. 8, pp107–129*. eds. P. Olson.

Labrosse, S. (2003). Thermal and magnetic evolution of the earth's core. *Physics of the Earth and Planetary Interiors*, 140(1):127–143.

Labrosse, S., Poirier, J.-P., and Le Mouël, J.-L. (1997). On cooling of the earth's core. *Physics of the earth and planetary interiors*, 99(1):1–17.

Lay, T. and Young, C. J. (1990). The stably-stratified outermost core revisited. *Geophysical Research Letters*, 17(11):2001–2004.

Liao, X., Zhang, K., and Earnshaw, P. (2001). On the viscous damping of inertial oscillation in planetary fluid interiors. *Physics of the Earth and Planetary Interiors*, 128(1):125–136.

Lister, J. R. and Buffett, B. A. (1998). Stratification of the outer core at the core-mantle boundary. *Physics of the earth and planetary interiors*, 105(1):5–19.

Malkus, W. V. (1967). Hydromagnetic planetary waves. *Journal of Fluid Mechanics*, 28(04):793–802.

Melchior, P. and Ducarme, B. (1986). Detection of inertial gravity oscillations in the earth's core with a superconducting gravimeter at brussels. *Physics of the Earth and Planetary Interiors*, 42(3):129–134.

Melchior, P. J., Crossley, D., Dehant, V., and Ducarme, B. (1988). *Have inertial waves been identified from the Earth's core?*, volume 46. American Geophysical Union.

Nakagawa, T. (2011). Effect of a stably stratified layer near the outer boundary in numerical simulations of a magnetohydrodynamic dynamo in a rotating spherical shell and its implications for earth's core. *Physics of the Earth and Planetary Interiors*, 187(3):342–352.

Olsen, N., Friis-Christensen, E., Floberghagen, R., Alken, P., Beggan, C. D., Chulliat, A., Doornbos, E., da Encarnação, J. T., Hamilton, B., Hulot, G., von den IJssel, J., Kushinov, A., Lesur, V., Lühr, H., Macmillan, S., Maus, S., Noja, M., Olsen, P. E. H., Park, J., Plank, G., Püthe, C., Rauberg, J., Ritter, P., Rother, M., Sabaka, T., Schachtschneider, R., Sirol, O., Stolle, C., Thébault, E., Thomson, A. W., Tøffner-Clausen, L., Velímský, J., Vigneron, P., and Visser, P. N. (2013). The swarm satellite constellation application and research facility (scarf) and swarm data products. *Earth, Planets and Space*, 65(11):1189–1200.

Olson, P. (1977). Internal waves in the earth's core. *Geophysical Journal International*, 51(1):183–215.

Pais, M. A. and Jault, D. (2008). Quasi-geostrophic flows responsible for the secular variation of the earth's magnetic field. *Geophysical Journal International*, 173(2):421–443.

Pozzo, M., Davies, C., Gubbins, D., and Alfè, D. (2012). Thermal and electrical conductivity of iron at earth's core conditions. *Nature*, 485(7398):355–358.

Rieutord, M., , and Valdettaro, L. (1997). Inertial waves in a rotating spherical shell. *Journal of Fluid Mechanics*, 341:77–99.

Rieutord, M. (1995). Inertial modes in the liquid core of the earth. *Physics of the Earth and Planetary Interiors*, 91(1):41–46.

Schaeffer, N. (2013). Efficient spherical harmonic transforms aimed at pseudospectral numerical simulations. *Geochemistry, Geophysics, Geosystems*, 14(3):751–758.

Schmitt, D. (2010). Magneto-inertial waves in a rotating sphere. *Geophysical and Astrophysical Fluid Dynamics*, 104(2-3):135–151.

Souriau, A. (2007). Deep earth structure—the earth's cores. *Treatise on Geophysics*, 1:655–693.

Takehiro, S. and Lister, J. (2002). Surface zonal flows induced by thermal convection trapped below a stably stratified layer in a rapidly rotating spherical shell. *Geophysical research letters*, 29(16):50–1.

Takehiro, S. I. and Lister, J. R. (2001). Penetration of columnar convection into an outer stably stratified layer in rapidly rotating spherical fluid shells. *Earth and Planetary Science Letters*, 187(3):357–366.

Zhang, K. (1993). On equatorially trapped boundary inertial waves. *Journal of Fluid Mechanics*, 248:203–217.

Zhang, K., Earnshaw, P., Liao, X., and Busse, F. (2001). On inertial waves in a rotating fluid sphere. *Journal of Fluid Mechanics*, 437:103–119.

Zhang, K., Liao, X., and Schubert, G. (2003). Nonaxisymmetric instabilities of a toroidal magnetic field in a rotating sphere. *The Astrophysical Journal*, 585(2):1124.

Zhang, K. and Schubert, G. (1997). Linear penetrative spherical rotating convection. *Journal of the atmospheric sciences*, 54(21):2509–2518.